

REPORTS

fact that monophosphorylated Rab:REP complexes appear to be more stable than the diphosphorylated species indirectly supports this assumption (23).

The structure provides a basis for analysis of disease-causing mutations in RabGDI, such as I100P (I92P in mammalian nomenclature), which leads to familial mental retardation in humans. This mutation is characterized by reduced Rab extraction from the membranes (7). gI100 is located in the CBR and is part of a group of nonpolar residues on the surface of the RabGDI molecule that form an extended hydrophobic patch with a central cavity on the lower part of domain II (Fig. 2A). This assembly is involved in binding of the C-terminus of Ypt1 via interaction with Val¹⁹¹ and Leu¹⁹³ and induces a 90° turn in the C-terminus, which directs it over the effector loop toward the lipid-binding site. Mutations in this hydrophobic patch are expected to have a twofold effect. First, they will impair C-terminus binding and will reduce the affinity of the RabGDI molecule for Ypt. Second, and possibly more important, they will perturb the orientation of the Ypt C-terminus in the vicinity of the effector loop and the lipid-binding domain. This is likely to interfere with GTPase interaction with molecules assisting delivery and removal of Rab proteins to and from the membrane. Consistent with this model, mutations in residues Thr¹⁰⁵ and Tyr²²⁷, which are part of the same hydrophobic patch, were also shown to interfere with membrane extraction of Ypt/Rab proteins (22, 24). Therefore, the α -RabGDI mutation I92P associated with mental retardation compromises the interaction with the peptide part of the C-terminus, and not the integrity of the isoprenoid-binding site, as initially proposed (9).

The structure also provides additional insights into the mechanism of RabGDI-mediated delivery of Rab proteins to the membranes. At least three structural elements of the complex were proposed to regulate loading of Rab proteins onto membranes: the hypervariable region of the Rab C-terminus, the conjugated isoprenoids, and the effector loop of RabGDI (4, 16, 25). All these elements are closely associated and well exposed in the Ypt1:RabGDI complex, making them clearly accessible to the putative membrane receptor (Figs. 1A and 2A).

In summary, we suggest a model in which RabGDI initially recognizes the globular core domain of the Rab/Ypt molecule by the Rab-binding platform interaction with switch I and II regions. This relatively low affinity binding is followed by interaction of the initially disordered C-terminus with the hydrophobic patch of the CBR. This stabilizes the interaction of domain II of RabGDI with the membrane over the buried geranylgeranyl moieties. A conformational change leads to opening of the hydrophobic cavity between helices D and E in domain II and facilitates extraction

of the first geranylgeranyl lipid from the bilayer (Fig. 4). The second lipid follows and is accommodated in the vicinity of the first lipid-binding site. This mechanism helps to explain the detrimental effect of mutations leading to weaker binding of the Rab C-terminus.

Reference and Notes

1. S. R. Pfeffer, *Trends Cell Biol.* **11**, 487 (2001).
2. N. Segev, *Curr. Opin. Cell Biol.* **13**, 500 (2001).
3. M. Zerial, H. McBride, *Nature Rev. Mol. Cell Biol.* **2**, 107 (2001).
4. C. Alory, W. E. Balch, *Traffic* **2**, 532 (2001).
5. In the protein, Ile⁹² is replaced by Pro (I92P). Single-letter abbreviations for the amino acid residues are as follows: A, Ala; C, Cys; D, Asp; E, Glu; F, Phe; G, Gly; H, His; I, Ile; K, Lys; L, Leu; M, Met; N, Asn; P, Pro; Q, Gln; R, Arg; S, Ser; T, Thr; V, Val; W, Trp; and Y, Tyr.
6. M. D. Garrett, J. E. Zahner, C. M. Cheney, P. J. Novick, *EMBO J.* **13**, 1718 (1994).
7. P. D'Adamo *et al.*, *Nature Genet.* **19**, 134 (1998).
8. I. Schalk *et al.*, *Nature* **381**, 42 (1996).
9. Y. An *et al.*, *Structure (Cambridge)* **11**, 347 (2003).
10. H. Horiuchi, O. Ullrich, C. Bucci, M. Zerial, *Methods Enzymol.* **257**, 9 (1995).
11. A. Kalinin *et al.*, *Protein Expr. Purif.* **22**, 84 (2001).
12. K. Alexandrov *et al.*, *J. Am. Chem. Soc.* **124**, 5648 (2002).
13. B. Ludolph, F. Eisele, M. Waldeman, *J. Am. Chem. Soc.* **124**, 5954 (2002).
14. T. W. Muir, *Annu. Rev. Biochem.* **72**, 249 (2003).
15. A. T. Constantinescu *et al.*, *Structure (Cambridge)* **10**, 569 (2002).
16. P. Chavrier *et al.*, *Nature* **353**, 769 (1991).
17. A. Rak, K. Alexandrov, unpublished observations.
18. P. A. Boriack-Sjodin, S. M. Margarit, D. Bar-Sagi, J. Kuriyan, *Nature* **394**, 337 (1998).

19. G. R. Hoffman, N. Nassar, R. A. Cerione, *Cell* **100**, 345 (2000).
20. O. Pylypenko *et al.*, *Mol. Cell* **11**, 483 (2003).
21. C. S. Ricard *et al.*, *Genesis* **31**, 17 (2001).
22. P. M. Gilbert, C. G. Burd, *J. Biol. Chem.* **276**, 8014 (2001).
23. F. Shen, M. C. Seabra, *J. Biol. Chem.* **271**, 3692 (1996).
24. T. Sakisaka, T. Meerlo, J. Matteson, H. Plutner, W. E. Balch, *EMBO J.* **21**, 6125 (2002).
25. P. Luan *et al.*, *Traffic* **1**, 270 (2000).
26. A. T. Brunger *et al.*, *Acta Crystallogr. D Biol. Crystallogr.* **54** (Pt. 5), 905 (1998).
27. G. Holtermann is acknowledged for invaluable technical assistance. We thank the staff of SLS beamline at Paul Scherrer Institute, Villigen, for help during data collection. We thank I. Schlichting and W. Blankenfeldt for help with data collection and A.-C. Ceacareanu for help with construction of expression vectors. D. Gallwitz is acknowledged for a generous gift of anti-Ypt1 antibody. W. Blankenfeldt is gratefully acknowledged for critically reading the manuscript and stimulating discussions. A.R. was supported by an Engelhorn foundation long-term postdoctoral fellowship. L.B. was supported by postdoctoral fellowship of the Alexander von Humboldt Foundation. This work was supported in part by grant DFG AL 484/5-2 to K.A. and grant I/77 977 of the Volkswagen foundation to K.A., R.S.G., and H.W. Coordinates have been deposited in the Protein Data Bank (Brookhaven National Laboratory) with accession number 1URV.

Supporting Online Material

www.sciencemag.org/cgi/content/full/302/5645/646/DC1
Materials and Methods
Figs. S1 to S3
Table S1
References and Notes
Movie S1

9 June 2003; accepted 5 September 2003

A New Class of Bacterial RNA Polymerase Inhibitor Affects Nucleotide Addition

Irina Artsimovitch,^{1*} Clement Chu,² A. Simon Lynch,^{2†} Robert Landick^{1†}

RNA polymerase (RNAP) is the central enzyme of gene expression. Despite availability of crystal structures, details of its nucleotide addition cycle remain obscure. We describe bacterial RNAP inhibitors (the CBR703 series) whose properties illuminate this mechanism. These compounds inhibit known catalytic activities of RNAP (nucleotide addition, pyrophosphorolysis, and Gre-stimulated transcript cleavage) but not translocation of RNA or DNA when translocation is uncoupled from catalysis. CBR703-resistance substitutions occur on an outside surface of RNAP opposite its internal active site. We propose that CBR703 compounds inhibit nucleotide addition allosterically by hindering movements of active site structures that are linked to the CBR703 binding site through a bridge helix.

Bacterial RNAPs typically consist of five polypeptides: β , β' , α , and ω . β' and β form a main channel that holds the RNA 3' OH in

¹Department of Bacteriology, University of Wisconsin, Madison, WI 53706, USA. ²Cumbre Inc., 1502 Viceroy Drive, Dallas, TX 75235, USA.

*Present address: Department of Microbiology, Ohio State University, Columbus, OH 43210, USA.

†To whom correspondence should be addressed. E-mail: simon.lynch@cumbre.net (A.S.L.); landick@bact.wisc.edu (R.L.)

the active site, an 8 to 9 base pair RNA:DNA hybrid, duplex DNA in front of the hybrid, and single-stranded RNA upstream from the hybrid. A secondary channel connects the active site to the surrounding solution and may serve as a passageway for entering nucleoside triphosphates (NTPs), exiting pyrophosphate, or both. Within the main channel, bacterial and eukaryotic RNAPs are nearly identical in structure; thus, the mechanism of transcription by the multisubunit RNAPs of

all cellular life forms appears to be the same (1, 2). Nucleotide addition occurs by two Mg²⁺-catalyzed second-order nucleophilic displacement (S_N2) of the RNA 3' OH on the α phosphate of a NTP; the 3' nucleotide and the NTP are bound in subsites *i* and *i*+1,

respectively. Steps in the cycle of NTP entry, catalysis, and translocation of the 3' nucleotide from *i* to *i*+1 are thought to require movements of active site structures, in particular a long α helix that spans the main channel in front of the active site, called the F

or "bridge" helix (3–5). The precise nature of these movements is unknown.

Four inhibitors of RNAP are well characterized, although many others are known. Rifampicin binds bacterial RNAP in a pocket that contacts nascent RNA in transcription elongation complexes (TECs). Rifampicin blocks synthesis of RNAs longer than 2 to 3 nucleotides but cannot bind to or inhibit TECs (6). α-amanitin binds within the secondary channel of eukaryotic RNAPII, where it contacts the bridge helix and a coiled coil at the outer rim of the secondary channel (the funnel helices). α-amanitin inhibits nucleotide addition at all stages of transcription, possibly by restricting movement of the bridge helix, partially blocking the secondary channel, or both (7). Many amino acid substitutions confer resistance to rifampicin or α-amanitin; importantly, all occur in the inhibitor binding sites (6, 7). Other substitutions identify overlapping but distinct binding sites near the secondary channel and active sites for streptolydigin and microcin J25, which affect bacterial RNAP similarly to α-amanitin's effect on RNAPII (8, 9).

We isolated a new class of bacterial RNAP inhibitor by screening a large library of compounds for inhibition of transcription by *Escherichia coli* RNAP (10). The progenitor compound, C0340703 (*N*-hydroxy-*N'*-phenyl-3-trifluoromethyl-benzamidine) (Fig. 1A), is hereafter designated "CBR703." Variants of CBR703 were synthesized that gave increased potency, including CBR9379 (3-[3-

Fig. 1. CBR703 inhibitors of bacterial RNAP. (A) Chemical structures of relevant inhibitors from the CBR703 series. CBR703, CBR9379, and CBR9393. (B) Inhibition of *in vitro* transcription by the CBR703 class of inhibitors. Wild-type and mutant RNAPs were prepared from strains that overexpress RNAP (17). Inhibitors were added at increasing concentrations to reactions containing 30 nM wild-type or mutant RNAP, 25 nM T7 A1 promoter-containing DNA template, 50 μM ApU dinucleotide, and 10 μM each of ATP, GTP, and [α-³²P]CTP. After separation of the A29 RNA in a denaturing polyacrylamide gel (inset), the quantity of halted A29 RNA formed after 10 min, relative to the amount produced without inhibitor, was measured and plotted as a function of CBR703 inhibitor concentration (plot for CBR9379 shown; symbols defined in table at right). High concentrations of the CBR703 class of inhibitors only partially blocked the activity of some mutant RNAPs; therefore, both a residual activity and concentration of the inhibitor that produced half-maximal effect (IC₅₀) were determined.

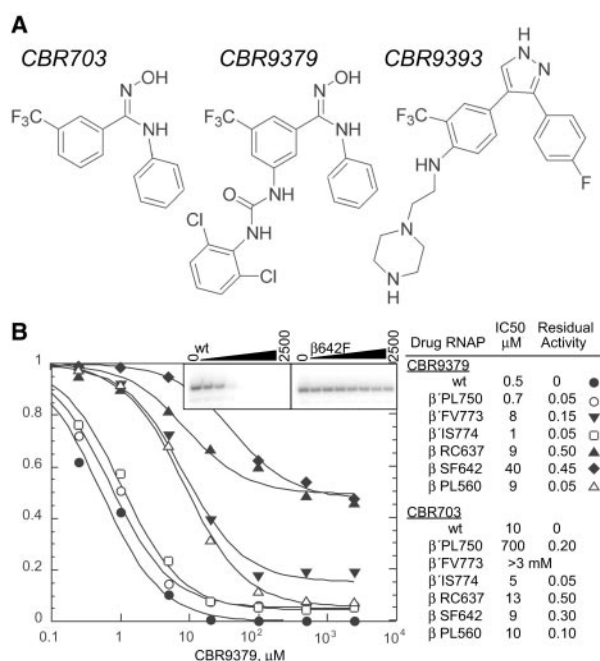
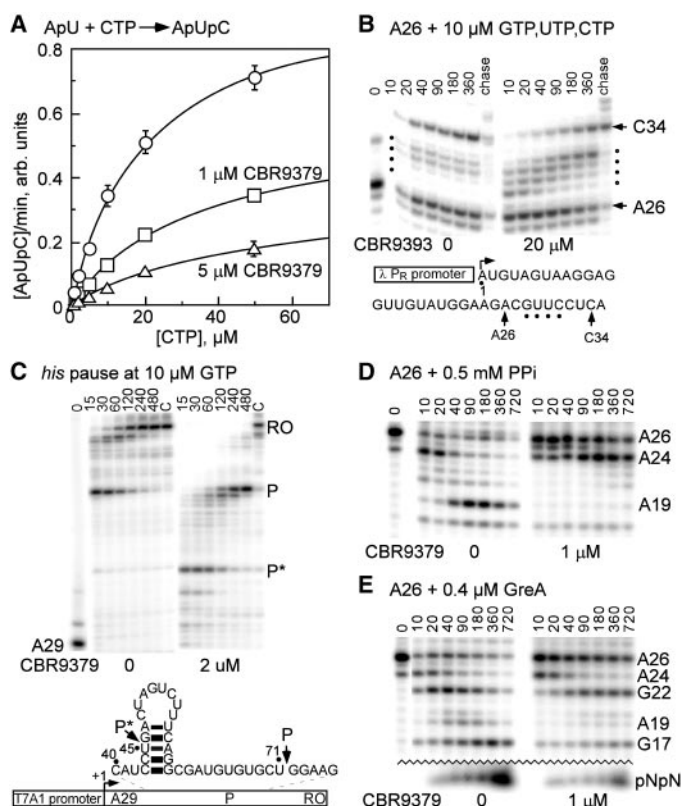


Fig. 2. Effect of the CBR703-type inhibitors on different stages of transcription. (A) Effect of CBR9379 on initiation. ApUpC was formed from ApU dinucleotide (150 μM) and [α-³²P]CTP using open complexes formed by *E. coli* RNAP on a T7 A1 promoter DNA (40 nM each) in a standard abortive initiation assay (10 min, 37°C) (13). ○, no inhibitor; V_{max}^{app} = 1.0 ± 0.03; K_{CTP} = 20 ± 1 μM. □, 1 μM CBR9379; V_{max}^{app} = 0.59 ± 0.03; K_{CTP} = 35 ± 3 μM. △, 5 μM CBR9379; V_{max}^{app} = 0.36 ± 0.02; K_{CTP} = 49 ± 4 μM. (B) Effect of CBR9393 on transcript elongation. A26 TECs immobilized on Ni²⁺-NTA (nitrilotriacetic acid) agarose were formed on a λ P_R DNA template using His₆-tagged RNAP by standard methods (14) and were then allowed to elongate the RNA transcript for the times indicated with 10 μM CTP, UTP, and GTP in the absence or presence of 20 μM CBR9393. The 10-s lane without CBR9393 was underloaded. (C) Effect of CBR9379 on transcriptional pausing. A29 TECs were formed on a T7 A1 promoter-*his* pause DNA template and were then allowed to elongate the RNA transcript at 10 μM GTP with 150 μM each of ATP, GTP, and CTP using standard methods (15). P, *his* pause RNA. RO, run-off RNA. P*, U45 pause activated by CBR9379. (D) Effect of CBR9379 on pyrophosphorolysis of A26 RNA at 0.5 mM PPI, as described (24, 25). (E) Effect of CBR9379 on GreA-stimulated hydrolysis of nascent RNA in A26 TECs, at 0.4 μM GreA as described (24, 25). The RNAs labeled pNpN are a heterogeneous set of cleavage products (typically dinucleotides) that accumulates near the bottom of the gel as cleavage proceeds (the jagged line indicates where a portion of the gel image was removed to conserve space).



REPORTS

(2,6-Dichloro-phenyl)-ureido]-*N*-hydroxy-*N'*-phenyl-5-trifluoromethyl-benzamidine) and CBR9393 ({4-[3-(4-Fluoro-phenyl)-1*H*-pyrazol-3-yl]-2-trifluoromethyl-phenyl}-(2-piperazin-1-yl-ethyl)amine) (Fig. 1A) (10). To verify the cellular target of CBR703 and to locate its binding site, we isolated derivatives of *E. coli tolC* strains that became resistant to CBR703 (10). These mutations were mapped to clusters near the middles of the *rpoB* and *rpoC* genes (encoding β and β' , respectively). Growth of some CBR703-resistant strains also proved to depend on CBR703; suppressor mutations that restored CBR703-independent growth affected nearby amino acids (figs. S1 and S2; table S1).

To verify that CBR703 directly inhibited RNAP, we purified both wild-type *E. coli* RNAP and RNAPs carrying the CBR703-resistance substitutions using an overexpression system for *E. coli* RNAP (11). We found that CBR703 directly inhibited RNA synthesis by RNAP in vitro, that the mutant RNAPs were resistant to significantly greater concentrations of CBR9379 than was wild-type RNAP, and that the sensitivity of RNAP to CBR703 derivatives paralleled their inhibition of growth of *E. coli tolC* strains (Fig. 1B). These results establish that bacterial RNAP is the cellular target of CBR703 and related inhibitors.

We then asked which step in the transcription cycle was affected by the CBR703-type inhibitors. CBR703 did not affect formation of promoter complexes by RNAP (12). To examine initiation of RNA synthesis, we looked for inhibition of CTP (cytidine triphosphate) reaction with ApU dinucleotide in T7 A1 promoter complexes [ApUpC is formed in a single-turnover, steady-state reaction and is released when the next required NTP, GTP (guanosine triphosphate), is absent (13)]. CBR9379 inhibited ApUpC formation even at high concentrations of CTP (Fig. 2A). This is consistent with noncompetitive, allosteric inhibition; however, the complex nature of the RNAP catalytic cycle precludes rigorous interpretation of these steady-state kinetics.

To determine whether the CBR703-type compounds inhibit nucleotide addition during transcript elongation, we tested their effect on preformed, immobilized TECs [A26 complexes halted on a λ P_R template (14)]. Upon addition of NTPs without inhibitor, RNAP paused before addition of C31 and C32 (Fig. 2B). Inclusion of CBR9393 slowed these steps, but more dramatically inhibited addition of U29 and U30. Thus, CBR9393 preferentially slows nucleotide addition at certain template positions. Most transcripts were extended upon addition of high concentrations of NTPs [chase (Fig. 2B)], and the effect of CBR9379 was eliminated by washing CBR9379-treated A26 TECs with buffer

(12). Thus, CBR9393 reversibly inhibits nucleotide addition but does not covalently modify RNAP or dissociate the TEC. (RNAP is incapable of elongating transcripts once they are released.)

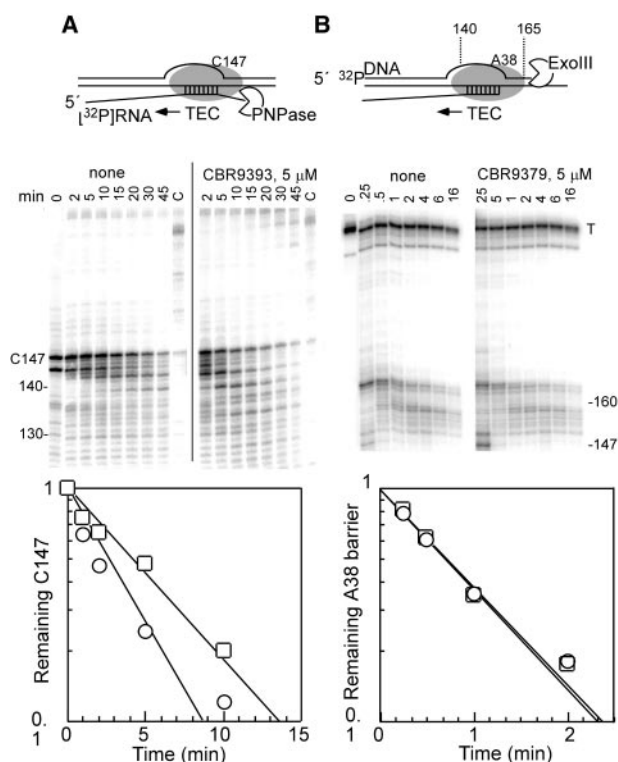
The preferential effect of the CBR703-type inhibitors at certain template positions also was evident during transcription of a template encoding the well-characterized *his* pause site (15) (Fig. 2C). CBR9379 both greatly slowed escape from the *his* pause site and activated a weak pause before addition of U45 on this template. Thus, CBR703-type compounds inhibit nucleotide addition at certain template positions, which often are positions at which the 3' RNA nucleotide is uridine; 3' uridine reacting with a purine NTP is, on average, the slowest nucleotide addition catalyzed by *E. coli* RNAP (16).

CBR703-type inhibitors could block any step in nucleotide addition: NTP-binding, catalysis, translocation of RNAP along DNA, or translocation of RNA from the *i*+1 to the

i site (the two translocation steps likely are obligatorily coupled). To determine whether they inhibit catalysis rather than NTP binding, we tested two reactions in which RNAP's catalytic cycle is reversed: pyrophosphorolysis (Fig. 2D) and GreA-stimulated hydrolytic cleavage of nascent RNA in RNAP's active site (Fig. 2E). Both reactions were inhibited by low concentrations of CBR9379. Thus, CBR703-type compounds inhibit all known catalytic functions of RNAP, even those that should not be affected by direct inhibition of NTP binding.

To determine whether CBR703-type inhibitors affect translocation of RNAP, we examined their effect on reverse translocation of RNAP uncoupled from catalysis [backtracking (17, 18)] using two approaches. First, we measured the rate at which polynucleotide phosphorylase (PNPase) shortened nascent RNA protruding from the downstream side of a backtracked TEC. PNPase removes single nucleotides from a RNA 3'

Fig. 3. Effect of the CBR703 class of inhibitors on reverse translocation by RNAP (gray oval). **(A)** Reverse translocation monitored by PNPase digestion of C147 nascent RNA. C147 TECs were formed as described previously (17), gel-filtered to remove NTPs, and then incubated at 37°C for the times indicated in a solution of 20 mM Tris-HCl, pH 7.9, 20 mM NaCl, 5 mM MgCl₂, 5% glycerol, 10% DMSO (dimethyl sulfoxide), 0.1 mM DTT (dithiothreitol) containing 1 mM sodium phosphate, PNPase (Sigma, St. Louis, MO catalog #P6264) at 0.25 U/ml, and CBR9379 inhibitor where indicated (more highly purified samples of PNPase did not work in this assay; the Sigma PNPase preparation lost substantial activity during storage for several months). A sample taken at the last time point was incubated with 500 μ M of each NTP for 5 min (lane C). No RNA shortening was observed in the absence of added phosphate. Initial rates of backtracking, as reflected by C147 RNA disappearance, were $1.7 \pm 0.2 \times 10^{-1} \text{ min}^{-1}$ without CBR9379 (\square) and $3.4 \pm 0.3 \times 10^{-1} \text{ min}^{-1}$ with CBR9379 (\circ). PNPase cleaved purified C147 RNA at an initial rate of $1.2 \pm 0.2 \times 10^{-1} \text{ min}^{-1}$ with or without CBR9379 (the slower cleavage of free RNA may reflect a higher concentration of free RNA relative to TECs, or RNA structure that inhibits PNPase access, but absent when RNA emerges from a TEC; data not shown). **(B)** Reverse translocation monitored by exoIII digestion of A38 nontemplate DNA strand. A38 TECs were formed on a ³²P-labeled linear template derived from pIA349 (11) in 20 mM Tris-HCl, pH 7.9, 20 mM NaCl, 5 mM MgCl₂, 0.1 mM DTT, and 5% glycerol in the presence of the Eco RI^{EQ111} roadblock protein bound to the upstream end of the template (26, 27). After addition of 10% v/v (volume for volume) DMSO or CBR9379 (in DMSO), exoIII (Boehringer Mannheim) was added to 0.025 U/ μ l and the reaction was incubated at 37°C for the times indicated. Based on the first four data points, the rates of backtracking sufficient to allow cleavage of nontemplate DNA past the initial barrier to exoIII digestion were $9.8 \pm 0.4 \times 10^{-1} \text{ min}^{-1}$ without added CBR9379 (\square) and $9.6 \pm 0.5 \times 10^{-1} \text{ min}^{-1}$ with CBR9379 (\circ) present.



terminus by reaction with inorganic phosphate (P_i) to yield nucleoside diphosphates. We formed halted TECs that contain a 147-nt G-less RNA and that backtrack readily (17), and we incubated them with PNPase and P_i after removal of NTPs by gel filtration (Fig. 3A). The rate of nascent RNA cleavage varied among batches of PNPase, suggesting it depended in part on impurities in the preparations. However, three aspects of the results were reproducible. First, cleavage depended on the presence of P_i . Second, addition of NTPs allowed re-extension of the shortened RNAs, verifying that they were still present in active TECs. Third, rather than inhibiting reverse translocation, CBR9379 increased the rate of RNA shortening \sim twofold.

We also examined the rate at which a $3' \rightarrow 5'$ processive exonuclease III (exoIII) shortened the nontemplate DNA strand in A38 TECs (11) formed on a modified T7 A1 promoter template (Fig. 3B). The rate of

backtracking was 3 to 6 times faster than observed by PNPase cleavage, possibly because exoIII acts on TECs backtracked by fewer nucleotides than PNPase, which cannot access RNA until it emerges from the secondary channel. For exoIII, the rate of backtracking was unaffected by CBR9379. Thus, the CBR703 inhibitor class does not affect translocation of either RNA or DNA through RNAP.

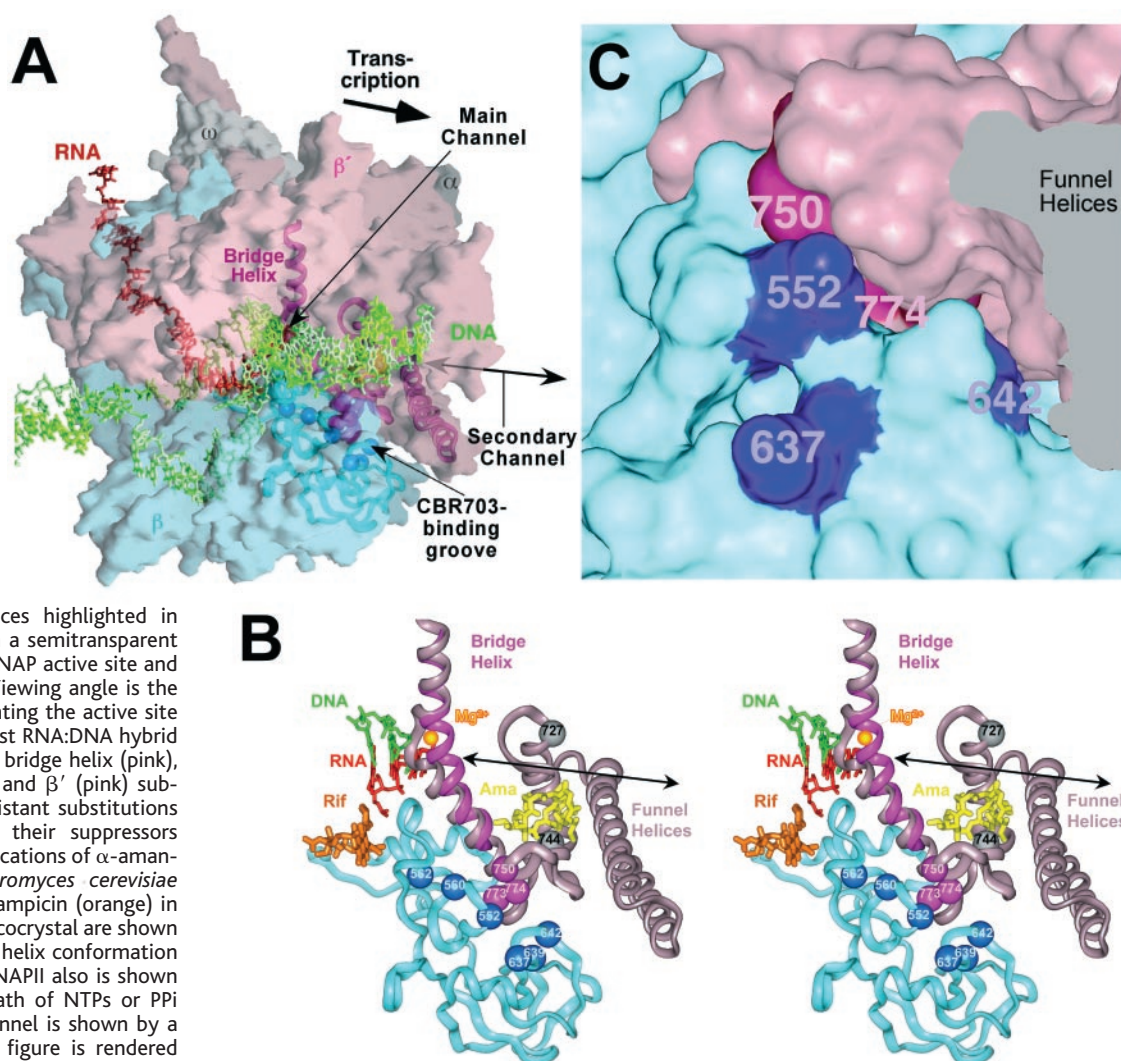
A putative binding site for the CBR703 class of inhibitors is defined by the location of amino acid changes that yield resistance (Fig. 4). CBR703 appears to bind to a surface-exposed groove at the junction of the β' bridge helix and the β subunit. This site is distinct from all known inhibitor binding sites on RNAP. The pattern of resistance substitutions suggests distinct pockets, which could contact the different planar rings of CBR703 (Fig. 4C). Because CBR703 inhibited nucleotide addition but not translocation, the effect

of bound CBR703 must be communicated from this surface-exposed binding site to the active site (Fig. 4B). Thus, CBR703 appears to be an allosteric inhibitor, blocking nucleotide addition without sterically occluding either the main channel or the secondary channel of the enzyme.

We propose that CBR703-type compounds inhibit RNAP because their interactions with the surface-exposed part of the bridge helix prevent the helix from assuming a conformation that is required for nucleotide addition. The bridge helix is known to be conformationally flexible; it and a nearby structural element called the trigger loop assume different interdependent conformations in different RNAP crystals (1–4). A bridge-helix distortion in one conformation occludes the $i+1$ site, and the trigger loop may block NTP binding in another, leading to proposals that these conformations could be involved in NTP binding (5) or translocation (3, 4). Al-

Fig. 4. Location of CBR703-resistant substitutions on RNAP. (A) Structure of a TEC based on the structure of *Thermus thermophilus* RNAP (4) adjusted by removal of α^A and the β' nonconserved region, inclusion of RNA and DNA strands based on TEC models and structures (3, 28), and adjustment of RNAP mobile domains (29) to the positions observed in a TEC structure (3). Subunits are colored as indicated below, and relevant features are labeled. The double-headed arrow indicates the path of the secondary channel, which opens to the active site from behind the surface of RNAP shown. The

locations of α -carbon traces highlighted in panel (B) are shown within a semitransparent RNAP. (B) Stereo view of RNAP active site and inhibitor-binding regions. Viewing angle is the same as in (A), but highlighting the active site Mg^{2+} (orange), three 3'-most RNA:DNA hybrid bp (DNA, green; RNA, red), bridge helix (pink), and segments of β (cyan) and β' (pink) subunits at which CBR703-resistant substitutions (cyan and magenta) and their suppressors (gray) occur (fig. S1). The locations of α -amanitin (yellow) in a *Saccharomyces cerevisiae* RNAPII cocystal and of rifampicin (orange) in a *Thermus aquaticus* RNAP cocystal are shown (6, 7). The alternate bridge helix conformation observed in *S. cerevisiae* RNAPII also is shown (magenta). The possible path of NTPs or P_i through the secondary channel is shown by a double-headed arrow. The figure is rendered for conventional stereoviewing. (C) Close-up view of the putative CBR703 binding groove in surface representation. To expose the groove, RNAP is rotated up 48°, left 17°, and counterclockwise 30° relative to the orientation in (A) and (B). Portions of the funnel helices are removed for clarity.



REPORTS

though CBR703 binding could block these steps allosterically, several arguments lead us to suggest that bound CBR703 inhibits a bridge-helix function in nucleotide addition. First, CBR703-type compounds do not inhibit reverse translocation (Fig. 3) and do inhibit catalytic events that do not require NTP binding (Fig. 2). Second, these compounds inhibit a single nucleotide-addition reaction that does not require translocation [ApU + CTP (Fig. 2A)]. Third, an ability of CBR703 to shift the energetics of bridge-helix conformations readily would explain how some substitutions make cells dependent on CBR703 for growth, whereas others outside the CBR703 binding site restore growth (figs. S1 and S2; table S1). Fourth, substitutions in the CBR703 binding site (e.g., β' FV773) substantially alter transcript elongation and pausing even when inhibitor is absent (12, 19). Finally, because particular sequences also may affect active site geometry (16, 20), this idea can explain why elongation at some template positions is especially sensitive to CBR703.

How bridge-helix and trigger-loop conformations facilitate nucleotide addition and how CBR703 compounds affect them remain to be determined. One possibility to consider is that bridge-helix deformation in the active site disrupts the helix dipole. Alternation between a deformed and continuous bridge helix could generate positive and negative charges at the active site proximal helix termini in the deformed conformation, which could be coupled to charge dynamics on NTP, PP_i, RNA, and DNA during nucleotide addition. CBR703 binding could reinforce or oppose these dynamics through interactions near the N-terminus of the bridge helix. Although this idea differs from the proposed role of the O-helix in DNA polymerases (21), it is consistent with previous proposals that an active site conformational change rate-limits DNA polymerases (22) and that conformational linkage exists between the active site of RNAP and a surface-exposed patch that includes the CBR703 binding site (19).

CBR703 compounds do not inhibit human RNAPII (23), which is not surprising because sequences around the CBR703 binding site are not conserved. Thus, systematic variation of the CBR703 structure informed by high-resolution structures of additional bacterial RNAPs holds great promise for rational design of drugs specifically targeted to major classes of bacterial pathogens.

References and Notes

1. P. Cramer, D. Bushnell, R. Kornberg, *Science* **292**, 1863 (2001).
2. G. Zhang *et al.*, *Cell* **98**, 811 (1999).
3. A. Gnatt, P. Cramer, J. Fu, D. Bushnell, R. D. Kornberg, *Science* **292**, 1876 (2001).
4. D. G. Vassylyev *et al.*, *Nature* **417**, 712 (2002).
5. V. Epshtein *et al.*, *Mol. Cell* **10**, 623 (2002).

6. E. A. Campbell *et al.*, *Cell* **104**, 901 (2001), and references therein.
7. D. A. Bushnell, P. Cramer, R. D. Kornberg, *Proc. Natl. Acad. Sci. U.S.A.* **99**, 1218 (2002), and references therein.
8. K. Severinov *et al.*, *J. Biol. Chem.* **270**, 23926 (1995).
9. J. Yuzenkova *et al.*, *J. Biol. Chem.* **277**, 50867 (2002), and references therein.
10. Materials and methods are available as supporting material on Science Online
11. I. Artsimovitch, V. Svetlov, K. Murakami, R. Landick, *J. Biol. Chem.* **278**, 12344 (2003).
12. I. Artsimovitch, unpublished results.
13. J. Smagowicz, K. Scheit, *Nucleic Acids Res.* **5**, 1919 (1978).
14. I. Artsimovitch, V. Svetlov, L. Anthony, R. R. Burgess, R. Landick, *J. Bacteriol.* **182**, 6027 (2000).
15. J. Ederth, I. Artsimovitch, L. Isaksson, R. Landick, *J. Biol. Chem.* **277**, 37456 (2002), and references therein.
16. V. A. Aivazashvili, R. S. Bibilashvili, R. M. Vartikyan, T. A. Kutateladze, *Mol. Biol.* **15**, 711 (1982).
17. G. Feng, D. N. Lee, D. Wang, C. L. Chan, R. Landick, *J. Biol. Chem.* **269**, 22282 (1994).
18. N. Komissarova, M. Kashlev, *Proc. Natl. Acad. Sci. U.S.A.* **94**, 1755 (1997).
19. T. Santangelo, R. Mooney, R. Landick, J. W. Roberts, *Genes Dev.* **17**, 1281 (2003).
20. C. L. Chan, R. Landick, *J. Mol. Biol.* **233**, 25 (1993).
21. S. Doublet, S. Tabor, A. M. Long, C. C. Richardson, T. Ellenberger, *Nature* **391**, 251 (1998), and references therein.
22. R. D. Kuchta, V. Mizrahi, P. A. Benkovic, K. A. Johnson, S. J. Benkovic, *Biochemistry* **26**, 8410 (1987).
23. M. Palangat, unpublished results.
24. I. Artsimovitch, L. C. Anthony, V. Svetlov, R. R. Burgess, R. Landick, *J. Bacteriol.* **182**, 6027 (2000).
25. I. Artsimovitch, R. Landick, *Proc. Natl. Acad. Sci. U.S.A.* **97**, 7090 (2000).
26. D. J. Wright, K. King, P. Modrich, *J. Biol. Chem.* **264**, 11816 (1989).
27. P. A. Pavco, D. A. Steege, *J. Biol. Chem.* **265**, 9960 (1990).
28. N. Korzheva *et al.*, *Science* **289**, 619 (2000).
29. S. A. Darst *et al.*, *Proc. Natl. Acad. Sci. U.S.A.* **99**, 4296 (2002).
30. Supported by grants from the Department of Agriculture (WIS04022) and NIH (GM38660) to R.L. and additional support from Cumbre, Inc., to I.A. and R.L.

Supporting Online Material

www.sciencemag.org/cgi/content/full/302/5645/650/DC1

Materials and Methods

Figs. S1 to S3

Table S1

References

2 June 2003; accepted 5 September 2003

Immune Control of Tuberculosis by IFN- γ -Inducible LRG-47

John D. MacMicking,^{1*} Gregory A. Taylor,^{2,3} John D. McKinney¹

Interferon- γ (IFN- γ) provides an essential component of immunity to tuberculosis by activating infected host macrophages to directly inhibit the replication of *Mycobacterium tuberculosis* (*Mtb*). IFN- γ -inducible nitric oxide synthase 2 (NOS2) is considered a principal effector mechanism, although other pathways may also exist. Here, we identify one member of a newly emerging 47-kilodalton (p47) guanosine triphosphatase family, LRG-47, that acts independently of NOS2 to protect against disease. Mice lacking LRG-47 failed to control *Mtb* replication, unlike those missing the related p47 guanosine triphosphatases IRG-47 or IGTP. Defective bacterial killing in IFN- γ -activated LRG-47^{-/-} macrophages was associated with impaired maturation of *Mtb*-containing phagosomes, vesicles that otherwise recruited LRG-47 in wild-type cells. Thus, LRG-47 may serve as a critical vacuolar trafficking component used to dispose of intracellular pathogens like *Mtb*.

Mycobacterium tuberculosis (*Mtb*) currently infects a third of the human population, claiming more lives each year than any other bacterial pathogen and rivaled only by the acquired immunodeficiency syndrome (AIDS) virus as a communicable cause of death (1). In developing countries, as many as 40 to 80% of individuals with AIDS will also develop tuberculosis (TB), indicating a key role for CD4⁺ T cells in

the immune control of *Mtb* infection (1, 2). CD4⁺ T cells secrete IFN- γ that in turn activates macrophages, the host cell in which *Mtb* chiefly resides and replicates, to inhibit bacterial growth (2). IFN- γ -induced expression of the antimicrobial enzyme NOS2 (3) is largely considered responsible for restricting *Mtb* replication via NO generation (4–6). Yet whether NOS2 accounts for all of the activity ascribed to IFN- γ has long been subject to debate (2, 3). This question takes on greater importance in light of three recent developments: (i) the choice of IFN- γ as a surrogate marker for vaccine efficacy and latent TB detection in humans (2, 7), (ii) the discovery of IFN- γ -related genetic mutations that predispose people to TB and other intracellular bacterial infections (8), and (iii) a realization that the response to IFN- γ is far more complex in mammals than was first envisaged (6, 9). Each development highlights

¹Laboratory of Infection Biology, Rockefeller University, 1230 York Avenue, New York, NY 10021, USA.

²Department of Medicine, Department of Immunology, Division of Geriatrics, and Center for the Study of Aging and Human Development, Duke University Medical Center, Durham, NC 27705, USA. ³Geriatric Research, Education, and Clinical Center, Durham Veterans Administration Medical Center, Durham, NC 27705, USA.

*To whom correspondence should be addressed. E-mail: macmicj@mail.rockefeller.edu